Multi-scale seasonal variability in Net Community Production and Chlorophyll in the Kuroshio Extension

Sophie Clayton[1], Hilary Palevsky[2], LuAnne Thompson[3], Paul Quay[3]

Corresponding author: Sophie Clayton (sclayton@odu.edu)

[1] Ocean, Earth and Atmospheric Sciences, Old Dominion University, Norfolk, VA, USA
[2] Department of Earth and Environmental Sciences, Boston College, Boston, MA, USA
[3] School of Oceanography, University of Washington, Seattle, WA, USA

Three key points:

1. *In situ* O_2/Ar data aggregated over three cruises reveal a hotspot of net community production to the north of the Kuroshio Extension Front.
2. The correlation between net community production, chlorophyll and sea level anomaly (a proxy for mesoscale eddies) varies regionally and seasonally.
3. In aggregate, a region of high net community production is associated with the Kuroshio nutrient stream, whereas chlorophyll varies with latitude.

Abstract

The Kuroshio current separates from the Japanese coast to become the Kuroshio Extension (KE) characterized by a strong latitudinal density front, high levels of mesoscale (eddy) energy, and high chlorophyll (CHL). Recent work has also shown that the KE carries subsurface nutrients into the region horizontally. While satellite measurements of CHL show evidence of the impact of eddies on the standing stock of phytoplankton, there have been very limited *in situ* estimates of productivity over synoptic scales in this region. Here, we present highly spatially resolved estimates of net community production (NCP) for the KE region derived from underway O_2/Ar measurements made in spring, summer, and early autumn. We find large seasonal differences in the relationships between NCP, CHL, and sea level anomaly (SLA, a proxy for local thermocline depth deviations driven by mesoscale eddies). The KE front is a pronounced hotspot of NCP in spring when NCP is almost completely decorrelated with CHL. Conversely, we find that NCP and CHL are strongly correlated in summer away from the front. We explore the mechanistic underpinnings of the relationship between NCP and CHL and suggest that the KE nutrient stream as well as vertical motions associated with mesoscale eddies might be a key factor in supporting an NCP hotspot that is seasonally decoupled from CHL at the KE front. Our observations also highlight seasonal and regional (de)coupling between NCP and CHL which may impact the accuracy of CHL-based estimates of productivity.

Plain Language Summary

Biological processes in the surface ocean play an important role in the ocean carbon cycle. Phytoplankton transform carbon dioxide into organic material, a portion of which then sinks into the deep where it can be stored long-term. This mechanism of carbon transfer from the surface to the deep ocean is known as the biological carbon pump. The processes that mediate this biological carbon pump can occur over short time and space scales. This is especially true in dynamic ocean systems such as western boundary currents where there are local maxima in weekly to interannual variability within the boundary current itself. Here we use novel continuous measurements made from ships of

opportunity to explore the variability in productivity and chlorophyll and how they are connected to physical ocean dynamics.

1. Introduction

The biological pump, the export of organic carbon from the surface to the deep ocean, plays a key role in the global carbon cycle. Inorganic carbon is converted to organic carbon by phytoplankton in the surface ocean through photosynthesis. A portion of this organic carbon is then exported from the surface and remineralized as it sinks through the water column, and is ultimately stored in the deep ocean with residence times of many months to centuries [*DeVries et al.*, 2012; *Giering and Humphreys*, 2018]. The processes that control the production, consumption, packaging, and export of organic carbon occur over relatively short time scales, from days to months, associated with biological processes, ecosystem dynamics and the evolution of the surface mixed-layer and mesoscale motions. More specifically, the time scales that control the production and export of carbon from the surface ocean span the division rate of phytoplankton cells O(1 day^{-1}), bloom events that last for weeks, and the seasonality of organic carbon production over the annual cycle in the mid and high latitudes. The spatial distribution of biogeochemical tracers in the surface ocean is also known to be very patchy, varying widely over scales as fine as O(<1km) [*Mackas et al.*, 1985; *van Gennip et al.*, 2016] up to basin scales O(1000km). This temporal and spatial variability presents a challenge to observing and understanding the drivers that control the production and export of organic carbon, particularly in highly dynamic ocean regions such as western boundary currents.

1.1 Measuring net community production in situ

Synoptic measurements of physical, chemical and biological parameters made at appropriate scales are necessary to understand the balance of processes that control rates of productivity and export. These types of measurements are also necessary to determine whether these processes are fully resolved, or at least well parameterized, in large-scale climate models used to make predictions about changes in ocean biogeochemical processes, and their impact on the global carbon cycle. However, measuring productivity *in situ* can be challenging as traditional bottle methods for estimating productivity rates are labor-intensive and do not allow for a large number of estimates to be made either at high resolution or synoptically over large areas. Remotely sensed productivity estimates can be made over large areas, but do not resolve fine scale variability and are subject to

85 substantial uncertainty [*Palevsky et al.*, 2016b]. As a result, although it is well-known
86 that phytoplankton standing stocks (e.g. measured by chlorophyll fluorescence, cell
87 counts and particulate organic carbon) are extremely patchy in time and space [*Mackas et*
88 *al.*, 1985], little is known about the scales of variability of rates of productivity and
89 export.
90
91 Non-incubation-based dissolved gas tracers have been used to derive synoptic, high-
92 resolution estimates of biological carbon export. Net community production (NCP, mmol
93 C m^{-2} day^{-1}) is the net sum of the organic carbon produced by gross primary production
94 (GPP, mmol C m^{-2} day^{-1}) and the organic carbon remineralised by respiration by both
95 heterotrophs (R_{HET}) and autotrophs (R_{PHY}) in the surface mixed layer:

96 $$NCP = \underbrace{GPP - R_{PHY}}_{NPP} - R_{HET} \quad (1)$$

97 where NCP values are positive in net autotrophic systems, and negative in net
98 heterotrophic systems. Net primary production (NPP) is the net sum of GPP and
99 respiration by phytoplankton. In steady state conditions with no transient change in the
100 surface biomass concentration, NCP represents the rate of organic carbon export from the
101 mixed layer. NCP can be estimated based on the biological supersaturation of dissolved
102 oxygen in the mixed layer, determined from the O_2/Ar dissolved gas ratio [*Craig and*
103 *Hayward*, 1987; *Emerson et al.*, 1991]. The development of continuous underway
104 methods to measure O_2/Ar [*Cassar et al.*, 2009; *Tortell*, 2005] has enabled new fine
105 spatial-scale estimates of NCP, which have been widely applied in both coastal and open
106 ocean regions [*Castro-Morales et al.*, 2013; *Estapa et al.*, 2015; *Eveleth et al.*, 2017; *R C*
107 *Hamme et al.*, 2012; *Izett et al.*, 2018; *Kaiser et al.*, 2005; *Lockwood et al.*, 2012;
108 *Manning et al.*, 2017; *Palevsky et al.*, 2013; *Rosengard et al.*, 2020; *Stanley et al.*, 2010;
109 *Tortell et al.*, 2014; *Tortell et al.*, 2011; *Ulfsbo et al.*, 2014]. The continuous and
110 simultaneous collection of underway measurements of dissolved gases, chlorophyll
111 fluorescence and physical ocean properties (e.g. temperature and salinity) allows us to
112 examine the relationship between physical and biogeochemical tracers. The high
113 temporal resolution of these continuous underway measurements also resolves variability
114 from the submesoscale (~1-10km) and mesoscale (~10-100km) to the basin scale.
115

1.2 A conceptual framework relating productivity, export and chlorophyll

The time rate of change of phytoplankton biomass is given by a balance between gross primary production and loss from grazing and export:

$$\frac{\partial P}{\partial t} = GPP - (R_{PHY} + R_{HET}) - export \quad (2)$$

where P is phytoplankton biomass (mmol C m^{-3}), GPP is the gross primary production (mmol C m^{-3} day^{-1}), R_{PHY} is the phytoplankton respiration rate (mmol C m^{-3} day^{-1}) and R_{HET} is respiration due to heterotrophy (mmol C m^{-3} day^{-1}). Phytoplankton biomass, P, can be related to CHL, which is more routinely measured, to derive an evolution equation for CHL:

$$\frac{\partial CHL}{\partial t} = [CHL: C][\mu(N, T, I) - R_{PHY}(T) - g(Z)]P - w_{bio}\frac{\partial P}{\partial z} \quad (3)$$

where CHL is related to P via C:CHL, the ratio of phytoplankton carbon (C) to CHL; μ is the phytoplankton growth rate (day^{-1}), which varies as a function of nutrient concentrations (N), temperature (T) and light (I); g(Z) is the zooplankton grazing rate (mmol C m^{-3} day^{-1}); and w_{bio} (m d^{-1}) is the sinking rate of phytoplankton cells. Whereas NCP represents the net sum of the rate processes that remove organic carbon from the surface mixed layer, CHL is a proxy for phytoplankton biomass modulated by the C:CHL ratio, also known to vary regionally and seasonally [e.g. *Westberry et al.*, 2016]. As a result of the significant variations in CHL:C in time and space, estimating $\frac{\partial P}{\partial t}$ from $\frac{\partial CHL}{\partial t}$ is subject to large uncertainties. Similarly, we might not expect CHL and NCP to vary in concert as NCP represents a rate of change of phytoplankton biomass, while CHL is a proxy for the biomass itself.

1.3 Productivity and export in the Kuroshio Extension

Western boundary current extensions are known to be regions of high open ocean productivity and are hypothesized to be hotspots of carbon export. These regions are characterized by both strong zonal currents and a strong density front. They are also characterized by energetic mesoscale and submesoscale dynamics that have been hypothesized to be strong drivers of primary production [*Mahadevan*, 2015] and export [*Honda et al.*, 2018]. As a result of this multi-scale variability in time and space, western

145 boundary current regions present a particular challenge to making observations that
146 resolve key biogeochemical processes [*Henson et al.*, 2016; *Todd et al.*, 2019].
147
148 The Kuroshio Extension (KE) is the branch of the Kuroshio western boundary current in
149 the Pacific, which turns to the east after separating off the coast of Japan. The seasonal
150 cycle of primary productivity in the KE region is relatively well known at specific
151 locations from moored time series studies. These studies show similar annual net
152 primary production (NPP) rates, obtained by ^{13}C incubations, both to the south and to the
153 north of the main KE front based on data collected at Station S1 (30°N, 145°E) in the
154 subtropical gyre, and Station K2 (47°N, 160°E) and the Kyodo North Pacific Ocean
155 Time-Series (KNOT, 44°N, 155°E) in the subarctic gyre, though with higher summer and
156 fall NPP to the north and higher winter and spring NPP to the south [*Imai et al.*, 2002;
157 *Matsumoto et al.*, 2016]. Although local time series studies are an important tool for
158 characterizing ocean biogeochemical processes, including the dynamics of the biological
159 carbon pump, they cannot fully describe the spatial variability found in the most dynamic
160 ocean regions [*Henson et al.*, 2016], thus these pointwise estimates of productivity are
161 difficult to extrapolate to generate accurate regional estimates of productivity, limiting
162 their utility.
163
164 The Kuroshio and Kuroshio Extension have been shown to act as a large-scale subsurface
165 nutrient stream, supporting large lateral transports of nutrients within the upper
166 thermocline [*Guo et al.*, 2013; *Guo et al.*, 2012]. The Kuroshio Extension is effective in
167 transporting nutrients in part because of large volume transports, but also because frontal
168 and mesoscale dynamics are associated with eddy scale vertical motions that can result in
169 anomalously high subsurface nutrient concentrations compared to adjacent waters along
170 the same isopycnals [*Nagai and Clayton*, 2017]. This suggests that the Kuroshio nutrient
171 stream injects nutrients into the surface mixed layer. Using satellite measured sea level
172 anomalies (SLA) and satellite estimates of CHL, *Kouketsu et al.* [2015] showed a
173 negative correlation between SLA and CHL concentrations in the Kuroshio Extension
174 region, suggesting that higher CHL is associated with cyclonic eddies. They also showed
175 seasonal differences in the strength of the correlations between SLA and CHL,

suggesting seasonal dynamics in the coupling between mesoscale eddies and CHL. However, *in situ* observational evidence that supports the role of mesoscale dynamics in nutrient delivery is still limited [*Clayton et al.*, 2014; *Nagai and Clayton*, 2017].

Here we analyze underway O_2/Ar derived estimates of *in situ* NCP spanning the KE region from three different seasons: May 2011, September 2011, and July 2012. We use satellite SLA data to identify eddy activity along the cruise tracks allowing us to we investigate the role of physical ocean dynamics in regional and seasonal variations in the relationship between NCP, SLA and CHL. In addition, the high alongtrack resolution allows us to examine the scales of variability and seasonal variations in NCP and surface CHL and the potential role of mesoscale eddies in fueling NCP. Finally, we examine the relationship between NCP and surface CHL and how this relationship varies by season. We find large seasonal differences in the correlation between NCP and surface CHL and show that they are strongly decoupled across all scales in spring when NCP is at its peak, but strongly coupled in summer away from the KE jet. Finally, we use the conceptual model in eqn. 3 to propose hypotheses for the observed (de)correlation in the distributions and variability of NCP and CHL, suggesting a (de)coupling in the processes controlling these quantities in the KE.

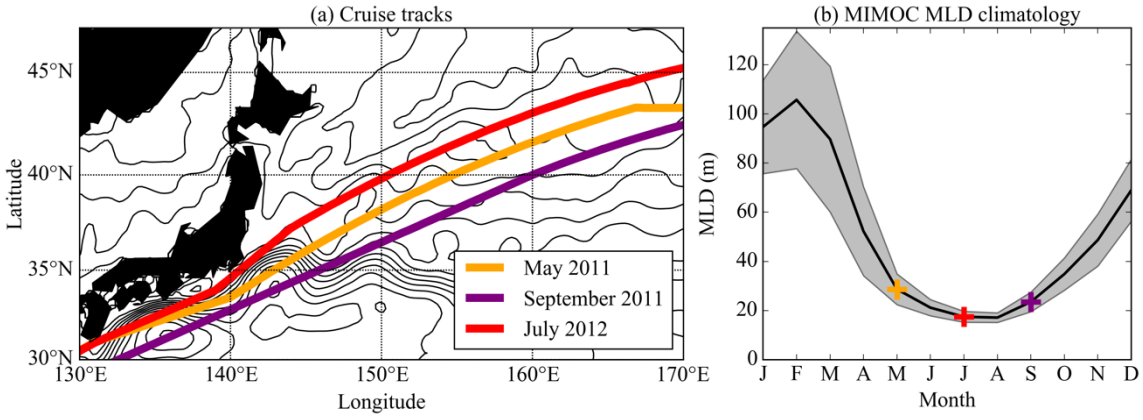

Figure 1. (a) Ship tracks for the three container ship cruises (May 2011, July 2012 and September 2011) shown over mean dynamic topography for the Kuroshio Extension region. (b) Climatological mixed layer depths for the study region bounded by 140°-170°E and 30°-45°N derived from the MIMOC data product. The months of each cruise are indicated by a colored cross.

2. Data and Methods

In this study we define the Kuroshio Extension sub-region of the North Pacific as the area bounded by 140° - 170°E and 30° - 45°N, following the definition in [*Palevsky et al.*, 2016b]. We combine data from several sources, described in detail below, including data collected underway from ships of opportunity (Figure 1a), remote sensing, repeat hydrographic surveys, and Biogeochemical-Argo floats.

2.1 Underway and discrete sampling for O_2/Ar and CHL

We continuously measured O_2/Ar dissolved gas ratios, temperature, salinity, and fluorescence from an underway seawater system (10 m depth) during basin-wide transects of the North Pacific on the M/V OOCL Tokyo (May and September 2011) and the M/V OOCL Tianjin (July 2012). For each transect, the containerships transited through the KE sub-region within approximately a week, resulting in synoptic measurements. Temperature and salinity were measured using a Sea-Bird Electronics SBE45 thermosalinograph. Fluorescence was measured using a Seapoint Chlorophyll Fluorometer and calibrated to calculate underway chlorophyll-*a* concentrations for each cruise based on discrete samples collected from the underway seawater line every 6-8 hours and measured following standard methods on a Turner fluorometer [*Strickland and Parsons*, 1972].

Underway measurements of O_2/Ar dissolved gas ratios were made using continuous flow equilibrator inlet mass spectrometry (EIMS), following the method of [*Cassar et al.*, 2009]. Water from the underway seawater system was pumped into an equilibrator cartridge (Membrana MicroModule G569, 0.75" x 1"), the headspace of which was delivered to a quadrupole mass spectrometer (Pfeiffer Prisma QMS) that measured individual ion currents at one-second intervals. Ion current ratios for O_2/Ar are reported as the mean over a three-minute measurement period, chosen to match the e-folding response time for this EIMS setup. This yields a spatial resolution of ~2 km at the average ship speed of ~25 knots. Thus, both mesoscale and submesoscale features are resolved. For the September 2011 cruise, a Loess filter with a 30-minute half-span was applied to remove high frequency instrument noise, reducing the spatial resolution to ~40

233 km, giving a marginal sampling for mesoscale fields. This filter was not applied to the
234 May 2011 or July 2012 cruises in order to preserve the spatial resolution of the data.
235
236 Seawater dissolved gas O_2/Ar ion current ratios from the mass spectrometer were
237 calibrated by first correcting for instrument drift based on measurements of atmospheric
238 O_2/Ar (a known standard) sampled for 30 minutes every 3 hours, and second by
239 calibrating to discrete seawater samples collected every 6-8 hours and measured by IR-
240 MS (see *Palevsky et al.* [2016a] for details of the discrete sample measurement
241 procedures). The discrete sample calibration used a time-varying correction factor based
242 on the weighted mean of the individual correction factors determined from the three
243 nearest discrete samples. Uncertainty in the final corrected O_2/Ar EIMS measurements,
244 determined based on comparison with the discrete IR-MS measurements, ranged from
245 0.4% to 1.0% across the three cruises.
246
247 NCP was calculated from measured O_2/Ar dissolved gas ratios using a simplified mixed
248 layer mass balance budget. The calculation assumes that, other than the biological effects
249 on O_2 owing to photosynthesis and respiration that we aim to quantify in calculating
250 NCP, air-sea gas exchange is the primary additional influence on mixed layer O_2 and Ar
251 concentrations.
252
253 $$\mathrm{NCP} = k[O_2]_{eq}\left(\frac{(O_2/Ar)_{meas}}{(O_2/Ar)_{eq}} - 1\right) \quad (4)$$
254
255 The subscript "meas" represents the measured values and the subscript "eq" represents
256 the temperature- and salinity-dependent concentrations of O_2 and Ar expected if the
257 mixed layer were in equilibrium with the atmosphere, calculated from the solubility of
258 both gases [*Garcia and Gordon*, 1992; *R Hamme and Emerson*, 2004]. *k* represents the
259 wind speed-dependent air-sea gas transfer velocity, calculated from daily wind speed data
260 from the NOAA National Climatic Data Center's multiple-satellite Blended Sea Winds
261 product (https://www.ncdc.noaa.gov/oa/rsad/air-sea/seawinds.html) following the
262 *Nightingale et al.* [2000] equation and the *Reuer et al.* [2007] time-dependent weighting
263 scheme. Final NCP values are converted to carbon units using an O_2: C photosynthetic

quotient of 1.4 [*Laws*, 1991]. Mean uncertainty in calculated NCP is 4.6 ± 2.3 mol C m^{-2} d^{-1}, determined by a Monte Carlo error analysis incorporating cruise-specific O_2/Ar measurement uncertainty and 14% uncertainty in the gas transfer velocity (as determined by *Palevsky et al.* [2016a]).

We omit from the mass balance budget additional terms accounting for physical advection, mixing, and transient changes due to non-steady state conditions over the dissolved gas residence time in the mixed layer. Although these processes can significantly influence the mixed layer O_2/Ar budget in cases with strong vertical exchange or deviations from steady state [*Jonsson et al.*, 2013], previous analysis of the mixed layer O_2/Ar budget over the seasonal cycle in the Kuroshio region of the North Pacific has shown that these influences are minimal during the period from springtime restratification through fall, the seasons chosen for analysis in this study [*Palevsky et al.*, 2016a].

2.2 Sea Level Anomaly data

In order to identify the location of the KE front and associated mesoscale eddies, we used 1/4° x 1/4° gridded daily sea level anomaly product that merges the data from multiple satellites to obtain a high-solution view of the dynamics of the upper ocean (the Ssalto/Duacs altimeter products produced and distributed by the Copernicus Marine and Environment Monitoring Service, CMEMS). Closed contours of sea level anomaly that enclose a hill/depression of sea level indicate the location of an anti-cyclonic/cyclonic (clockwise/anti-clockwise) eddy. There is an associated anomaly in thermocline depth that mirrors the SLA. For each cruise, we determined the date at which the cruise track crossed the KE front and used the SLA data for that day for our analysis of the linkages between NCP, CHL and SLA. For the May 2011, September 2011 and July 2012 cruises, we used SLA data obtained on 19/05/2011, 23/09/2011 and 27/02/2012, respectively. The container ships collecting the underway data crossed the region of interest within a 4- to 5-day period and we did not find any large changes in SLA within that time frame. In order to compare the higher resolution underway data to the satellite data, we binned and

294 averaged the underway data into each of the 1/4° x 1/4° SLA grid cells coinciding with
295 the ship tracks.
296
297 ***2.3 Nitrate data***
298 Samples for dissolved nutrient analyses were collected from the underway seawater line
299 at roughly the same frequency as the CHL samples, every 6-8 hours. These samples were
300 analyzed at the University of Washington Marine Chemistry Laboratory using standard
301 methods [*Intergovernmental Oceanography Commission*, 1994]. Although nutrient
302 samples were collected at the surface concurrently with the NCP and CHL data, these
303 data do not provide any information on the vertical structure of the nutrient fields in the
304 KE. The depth of the nutricline has been shown to vary considerably across the KE front
305 [*Clayton et al.*, 2014; *Nagai and Clayton*, 2017] and this is likely to be an important
306 control on vertical nutrient fluxes within the KE region. In order to understand possible
307 links between vertical nutrient fluxes and CHL and NCP, we make use of a range of
308 available, vertically resolved, *in situ* data collected between 2010 and 2017. This includes
309 data collected by Biogeochemical-Argo floats and Japan Meteorological Association
310 (JMA) repeat sections within the KE region in the period before and after our cruises.
311 The Biogeochemical-Argo nitrate data was downloaded directly from the MBARI
312 Chemical Sensor Group's FloatViz page (http://www.mbari.org/science/upper-ocean-
313 systems/chemical-sensor-group/floatviz/), and was comprised of measurements made by
314 two BGC-Argo floats, 7546 and 7674, both equipped with nitrate sensors and deployed in
315 the KE region in March 2013. Float 7564 and float 7674 continued collecting data until
316 early March 2017 and early January 2017, respectively. Only data from the floats flagged
317 as "good" was used in our analysis. In addition, we used data from the following JMA
318 cruises: 10-07 (October 2010), 11-08 (July – August 2011), 11-09 (September 2011), 12-
319 03 (April - May 2012), 12-05 (June – July 2012), 12-06 (July – September 2012), 13-04
320 (April – May 2013), 14-04 (April – May 2014), 15-04 (April – May 2015), 16-04 (April
321 – May 2016). Data from all of the JMA cruises are publicly available from the JMA data
322 portal (http://www.data.jma.go.jp/gmd/kaiyou/db/vessel_obs/data-
323 report/html/ship/ship_e.php).
324

During our study period, the KE took a zonal path, and was in its stable mode with no large-scale meander (e. g. Figure 3; *Qiu et al.* [2014]). The nitrate data from the sources listed above also corresponded to the KE's stable mode, thus allowing us to use that data to construct a composite section of the vertical structure of nitrate across the KE front. We excluded data collected during winter months (November, December, January and February) when the surface nutrient signals can be driven by deep winter mixing [*Wong et al.*, 2002]. Finally, we restricted the analysis to the top 150m of the water column in order to capture the spatial patterns in nitrate within the surface mixed layer and the top of the nutricline crossing the KE front.

2.4 Assessing spatial variability

Spatial variability for temperature, CHL and NCP from the May 2011 and July 2012 cruises was determined through a wavenumber Fourier transform. Because of the large instrument noise in the September 2011 cruise data, the data was not of high enough quality to determine variability at scales below ~80km, so it was excluded from this part of the analysis. The container ships maintained a relatively steady speed along the tracks, so the data are uniformly distributed in space, and we linearly interpolate the data onto a regular 2 km track. In order to focus on submesoscale and mesoscale variability, we split the data from each cruise into 500km overlapping segments, with 50 % overlap between adjacent segments. We then removed the linear trend from each segment and applied a Hanning window before performing the Fourier analysis. We normalized and averaged the spectra for all of the segments to obtain the mean spectrum for each full cruise track. We determine the 95% confidence interval in the spectra using the χ^2 distribution. The slope of the spectra, in the 5-20km and 20-200km wavelength ranges, is estimated by applying a linear regression to the log power spectral density estimates against the log of the wavelengths.

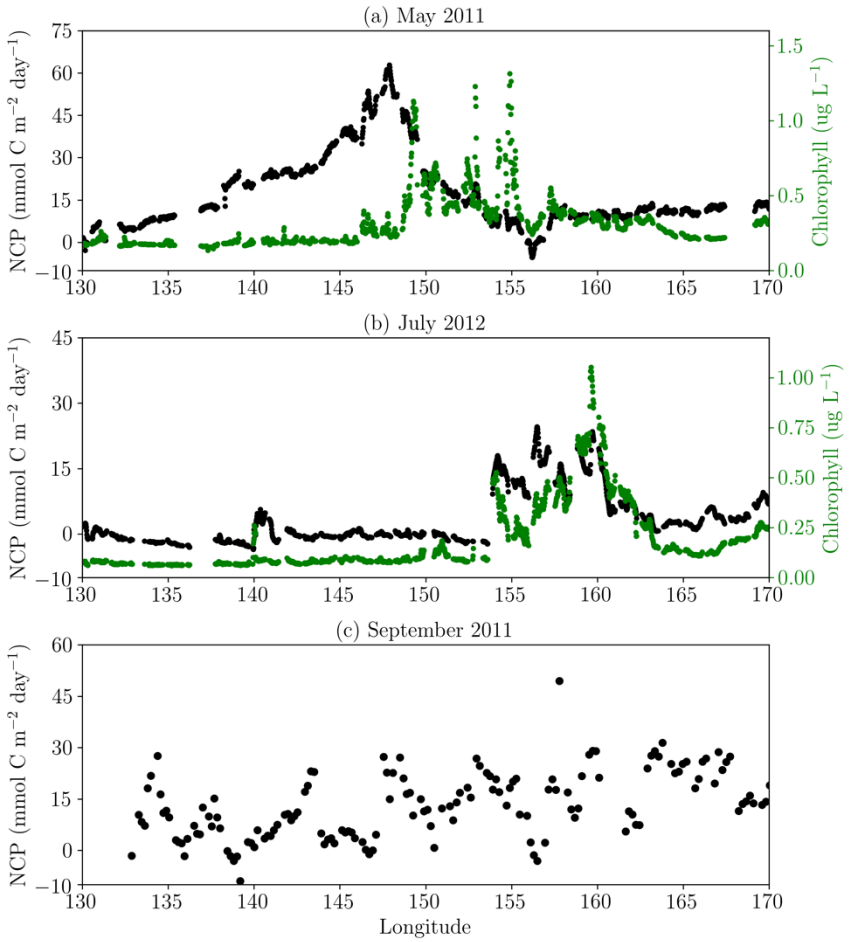

Figure 2. Underway surface estimates of NCP (mmol C m^{-2} d^{-1}) and surface CHL (µg L^{-1}), when available, for the (a) May 2011, (b) July 2012 and, (c) September 2011 cruises.

3. Results and Discussion

3.1. Physical setting and observed distributions of NCP and CHL

Each of the three container ship transects crossed the KE axis, with the May and September 2011 tracks both crossing the KE at approximately 145°E (Fig. 1a). The July 2012 transect was offset and crossed the Kuroshio front closer to the coast of Japan, largely bypassing the KE jet. Since the KE was in its stable mode with a shorter path length, a more northerly path, and relatively fewer mesoscale eddies [*Qiu et al.*, 2014], during the study period (May 2011 – July 2012), differences between May and September should be largely driven by seasonality, rather than differences in the level of mesoscale eddy activity. However, the transect in July was mostly to the north of the KE

axis. Although we do not have direct estimates of the mixed layer depth for our study period, we calculated the mean MLD over the study region from the Monthly Isopycnal & Mixed-layer Ocean Climatology (MIMOC; *Schmidtko et al.* [2013], Fig. 1b). The mean climatological MLDs over the study region are: 28.65 +/- 6.3 m, 17.46 +/- 2.2 m and 23.51 +/- 4.0 m in May, July and September, respectively with the uncertainty reflecting the variability across the region. From June to August, the MLDs are at their shallowest, while in May and September the MLDs are slightly deeper.

Table 1. Summary statistics for NCP (mmol C m^{-2} d^{-1}) and CHL (μg L^{-1}) data.

		Mean ± st. dev	Minimum	Maximum
May 2011	NCP	18.2 ± 14.2	-5.4	62.9
	CHL	0.4 ± 0.2	0.2	1.3
July 2012	NCP	4.6 ± 6.2	-2.3	24.6
	CHL	0.2 ± 0.2	0.1	1.1
September 2011	NCP	14.5 ± 9.9	-16.1	58.2
	CHL	--	--	--

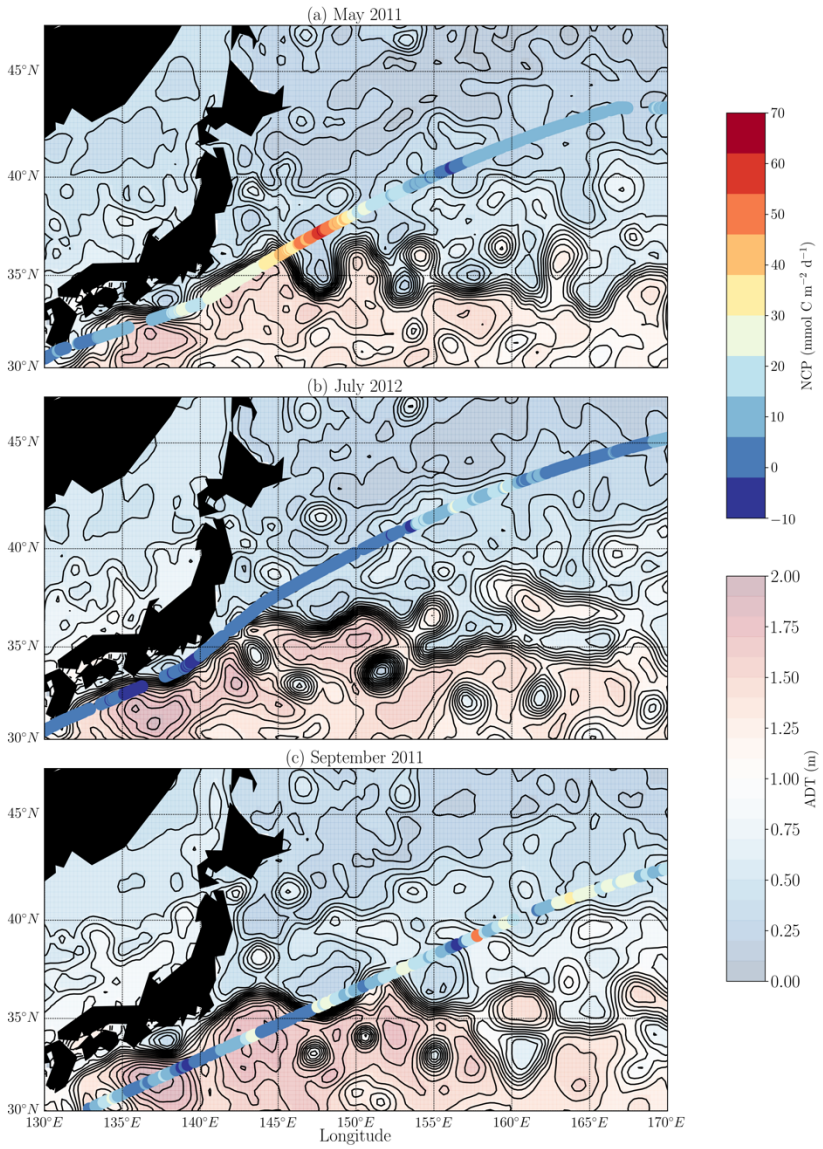

Figure 3. Daily maps of SLA with NCP overlain for the (a) May 2011, (b) July 2012 and, (c) September 2011 cruises. The mean dynamic topography is also indicated by black contour lines on each panel.

3.2 Correlations with SLA: influence of mesoscale processes on NCP and CHL

The correlation between SLA and NCP or CHL gives an indication of the importance of mesoscale features (particularly eddies) in driving the observed distributions of NCP and CHL. We examined correlations between SLA and NCP for each of the cruises individually (Table 2, Fig. 4). Overall, the highest NCP values are associated with low SLA (cyclonic cold-core eddies), however we did not find a consistent negative relationship between NCP and SLA as might be expected if NCP were suppressed when

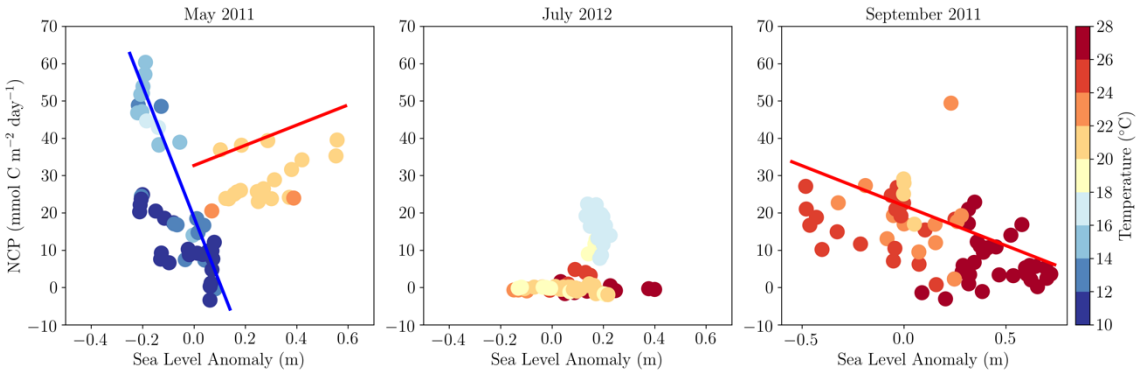

Figure 4. The relationship between SLA and NCP for the (a) May 2011, (b) July 2012 and, (c) September 2011 cruises. Regression lines are plotted on (a) for T > 18°C (red line) and T < 18°C (blue line); and on (c) for all points (black line).

the thermocline is deep. We found no significant relationship between NCP and SLA in the May 2011 data when analyzed over the full KE region. However, when the data was split into two subsets from north and south of the axis of the KE front, defined by temperatures greater than 18°C to the south and less than 18°C to the north, we found two distinct NCP vs. SLA regimes. South of the KE axis, with SST > 18°C, we found a moderate positive correlation between NCP and SLA (r = 0.44). North of the KE axis, with SST < 18°C, we found a strong negative correlation between NCP and SLA (r = -0.76). In the September 2011 data, we also found a moderate negative correlation between NCP and SLA (r = -0.50) over the entire cruise track, spanning both sides of the KE axis. For July 2012, where most of the data was collected to the north of the KE axis, we found a moderate positive correlation between NCP and SLA (r = 0.47). We also determined the correlation between CHL and SLA. In May 2011, we found a consistent moderate negative correlation between CHL and SLA (r = -0.48) across the full cruise track. In the July 2012 data, there was a moderate positive correlation between CHL and SLA (r = 0.36). Although fluorescence data was also collected during the September 2011 cruise, the fluorometer dynamic range was insufficient to obtain a good calibration with discrete samples, so we have excluded that data.

It is expected that cyclonic eddies, negative SLA features where the MLD and thermocline shoals and the nutricline is brought closer to the surface, should drive

increased primary production and enhanced CHL concentrations. Indeed, previous studies in the KE region have found negative correlations between SLA and satellite-derived CHL estimates. *Kouketsu et al.* [2015] found consistently negative correlations between SLA and CHL along and to the north of the KE main axis, but positive correlations between SLA and CHL in the recirculation gyre to the south of the KE axis. Some of our results are consistent with this previous work, however we also see positive correlations between both NCP and CHL and SLA in the July 2012 data, and a positive correlation between NCP and SLA in the warmer waters to the south of the KE axis in the May 2011 data. The highest NCP values seen in the July 2012 data are found within a region bounded by ~154°W and 165°W (Figure 3b), spanning roughly 600km of the cruise track. The Rossby radius of deformation in this region is ~30km [*Chelton et al.*, 1998], so this high NCP feature is far too large scale to be associated with mesoscale eddies. We also note that during the July 2012 cruise there was relatively low eddy activity such that SLA is small and not coherent (Figure 3b), suggesting that the high NCP north of the KE is related to the large scale circulation rather than mesoscale activity, possibly owing to the eastward flowing Oyashio Current that may bring nutrient coastal waters into the subarctic interior of the North Pacific [*Kono and Sato*, 2010]. This pathway is reflected by the mean SLA contours that originate near Hokkaido (the northernmost island in Figure 1a).

Table 2. Pearson correlation coefficients (r-values) for NCP and CHL with respect to SLA, and their respective p-values.

	Correlation coefficient	**p-value**
May 2011		
NCP	-0.11	0.38 (Not significant)
NCP (T>18°C)	0.44	< 0.05
NCP (T<18°C)	-0.76	< 0.05
CHL	-0.48	< 0.05
July 2012		
NCP	0.47	< 0.05
CHL	0.36	< 0.05
September 2011		
NCP	-0.50	< 0.05
CHL	--	--

While there is a negative correlation between SLA and CHL in the May 2011 data, the NCP relationship to SLA is different north and south of the front (Fig. 4). South of the KE axis, where CHL is high but NCP is relatively low (Figure 2a), the correlation between SLA and NCP is positive (Fig. 4). Conversely, north of the KE axis CHL is relatively low but NCP is high.

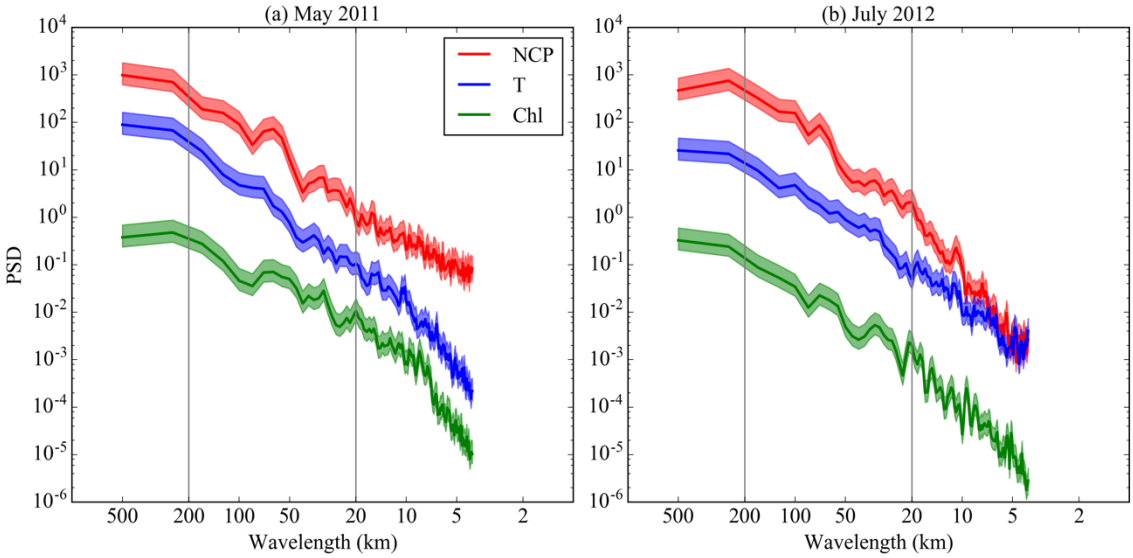

Figure 5. Normalised power spectral density (PSD) plotted against wavelength for NCP (blue), chlorophyll (green) and sea surface temperature (red) from underway data for the (a) May 2011 and (b) July 2012 cruises. The shaded area on each spectrum represents the envelope of the 95% confidence interval.

3.3 Spectral slopes of NCP, CHL and SST: mesoscale and submesoscale variability

We investigate the range and magnitude of spatial variability in temperature, CHL and NCP for the May 2011 and July 2012 cruises (Fig. 5). The September 2011 cruise data was excluded from this part of the analysis because the data was not of high enough spatial resolution to examine variance in the (sub)mesoscale range. Here, we examine the spectral slopes (α, the slope of log PSD vs. wavelength) for the mesoscale (20-200 km) and submesoscale range (5-20 km), reported in Table 3. Flatter spectral slopes (lower values of α) are diagnostic of higher variability at smaller wavelengths (smaller spatial scales). We find that values of α in the mesoscale range for all three tracers are similar in May and July. However, values of α in the submesoscale range in May and July diverge strongly between the three tracers. In May 2011, NCP has a much flatter spectrum in the

submesoscale range (α_{NCP} = -1.81) than temperature (α_T = -3.70) or chlorophyll (α_{CHL} = -4.01), indicating higher variability in NCP at smaller spatial scales. In the mesoscale range, NCP and temperature have similar spectra (α_{NCP} = -2.52 and α_T = -2.63), but chlorophyll has a much flatter spectrum (α_{CHL} = -1.66), indicating that chlorophyll has more spatial variability in the mesoscale range. In July 2011, NCP has a much steeper spectrum in the submesoscale range (α_{NCP} = -4.48) than temperature (α_T = -2.91) or chlorophyll (α_{CHL} = -3.22). In the mesoscale range in July, all of the tracers have similar spectral slopes (α_{NCP} = - 2.64, α_T = -2.36, and α_{CHL} = -2.05). These results suggest a consistent decoupling between NCP and both temperature and chlorophyll within the submesoscale range, with NCP having either much flatter or much steeper spectral slopes (α_{NCP}) in May and July, respectively. However, NCP and temperature appear to be more closely and consistently coupled in the mesoscale range, whereas chlorophyll consistently has a flatter spectral slope than both NCP and temperature in the mesoscale range.

Table 3. Spectral slopes for temperature, NCP and chlorophyll from the May 2011 and July 2012 cruises, with their respective r-values (all fits have p-values < 0.05).

	5 – 20 km range		20 -200 km range	
	Slope (α)	**r-value**	**Slope (α)**	**r-value**
May 2011				
NCP	-1.81	-0.93	-2.52	-0.95
Temperature	-3.70	-0.97	-2.63	-0.98
Chlorophyll	-4.01	-0.95	-1.66	-0.92
July 2012				
NCP	-4.48	-0.97	-2.64	-0.97
Temperature	-2.91	-0.95	-2.36	-0.97
Chlorophyll	-3.22	-0.93	-2.05	-0.93

Previous work has shown that both the reaction time (τ) and the scale of injection of a tracer can impact its spatial distribution, and therefore its spectral slope. Tracers with longer reaction times can be mixed down to smaller scales by the flow field, so tend to exhibit flatter spectral slopes [*Abraham*, 1998]. Additionally, the spatial scale of the processes that control the injection of a tracer, and whether or not it is related to the flow field also impacts its distribution. When the supply of a tracer is related to the structure of the flow field (e.g. eddies supplying nutrients to fuel production), then the spectral slope of the tracer tends to be flatter with more variance at fine scales [*Lévy and Klein*, 2004],

compared to when the tracer supply is uncorrelated with the flow field, in which case the spectral slope is controlled by the reaction time of the tracer [*Bracco et al.*, 2009].

In interpreting the spectral slopes reported here in Table 3, we must take into account fundamental differences in the controls on residence times of temperature, CHL, and O_2/Ar-based NCP. Sea surface temperature is largely controlled by ocean-atmosphere interactions and the thermal capacity of water, resulting in a residence time of ~30 days for temperature. We estimate the residence time for CHL to be on the order of 1-3 days given a characteristic phytoplankton cell doubling time of 1 day^{-1}. O_2/Ar-based NCP integrates over the dissolved gas residence time in the mixed layer (calculated as MLD/k). The mean dissolved gas residence times for study region for the May 2011 and July 2012 cruises, based on climatological MLD values and *k* (calculated as described in the Methods section), are 9.6 days and 4.4 days, respectively. Given these residence time estimates, in the simplest case where we assume that circulation features have no impact on tracer distributions, we might expect that NCP would always have a flatter slope than CHL (which has a shorter residence time) and a steeper slope than temperature (which has a longer residence time). However, we do not consistently observe these relationships between the temperature, CHL, and NCP spectral slopes. This indicates that coherent velocity structures in the flow field likely impact the spatial structure of the observed distributions of CHL and NCP, and may be diagnostic of localized vertical exchanges either injecting nutrients into or modifying the light field in the MLD, or localized areas of subduction removing organic carbon from the surface. Seasonal differences in the strength of submesoscale processes [*Rocha et al.*, 2016] might result in seasonal differences in the magnitude of the vertical supply of nutrients into the surface ocean. One interpretation of our results could be that there is a stronger submesoscale-driven vertical nutrient supply in May, when the mixed-layer is deeper than in July. Similarly, grazing will have an impact on both NCP and CHL variability, and heterotrophic respiration will also impact NCP variability.

We cannot test these hypotheses directly with this dataset, but future research should be designed to directly account for these processes. Understanding the individual and

combined effects of the gas residence time, nutrient inputs, grazing and coherent structures in the flow field on NCP spatial variability would be an important step in better constraining the impact of different processes on the observed temporal and spatial distributions of NCP.

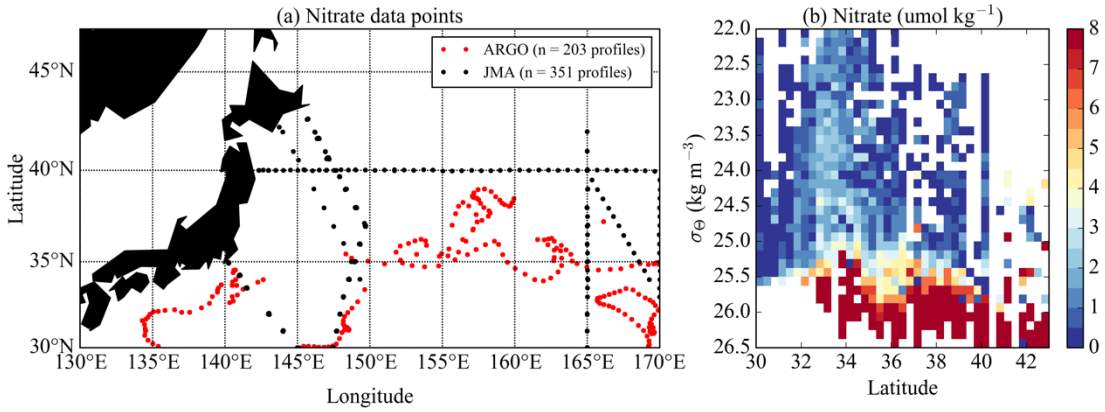

Figure 6. (a) Map of Biogeochemical-Argo and JMA profiles in the KE region from which nitrate depth profiles were used to construct the binned averages in panel (b). (b) Bin-averaged nitrate data in latitude vs. σ_t space. The data was limited to profiles made between April and October from the top 100m, to limit the influence of higher nutrient values driven by winter mixing.

3.4 Influence of the Kuroshio Extension nutrient stream on NCP and CHL

We examine the NCP data along with *in situ* nitrate data from Biogeochemical-Argo floats and JMA repeat sections from the KE region to discern whether regions where we would expect an enhanced supply of the nitrate to the euphotic zone due to the KE nutrient stream also support higher NCP. Although this *in situ* nitrate data was collected currently with the NCP measurements, the data is limited to a similar seasonal time range to the NCP data (April – October). We bin the *in situ* nitrate data into σ_t vs. latitude bins (Figure 6). We expect nitrate concentrations to be roughly constant along isopycnals, so a positive nitrate anomaly along isopycnals in the vicinity of the KE frontal axis is diagnostic of the nutrient stream. We find a positive anomaly in nitrate concentrations between 33°N and 36.5°N, and between the 23.5 kg m^{-3} and 25.5 kg m^{-3} isopycnals with respect to waters to the north and south (Figure 6). This confirms previous results based on a much finer scale survey of the KE that also found a nitrate anomaly in the same isopycnal range [*Nagai and Clayton*, 2017], within a 50km swath centered on the KE

axis. The main difference here is that we see the anomaly extending over a wider lateral range. This is likely because we incorporate data from a larger meridional and latitudinal range, spanning many months, whereas the previous survey took place over the course of 5 days over a much smaller region. The signature of the nutrient stream in our analysis of the *in situ* nitrate data, albeit over a wider latitudinal range suggests that the stream is a consistent feature of the KE that follows the KE axis as it moves meridionally. We combine and bin the NCP and CHL data in the same way as for nitrate (Figure 7), using CHL data from only the May 2011 and July 2012 cruises. We find that the highest CHL values tend to be found in denser, more northerly waters, in a density range from 24 kg m^{-3} to 26.5 kg m^{-3} and at latitudes north of 37°N. NCP has a different distribution, with the highest NCP values found in a density range 23.5 kg m^{-3} to 26.5 kg m^{-3}, and a latitudinal range from 35.5°N to 38.5°N. These elevated NCP values are found within a similar density and latitude range to the KE nutrient stream.

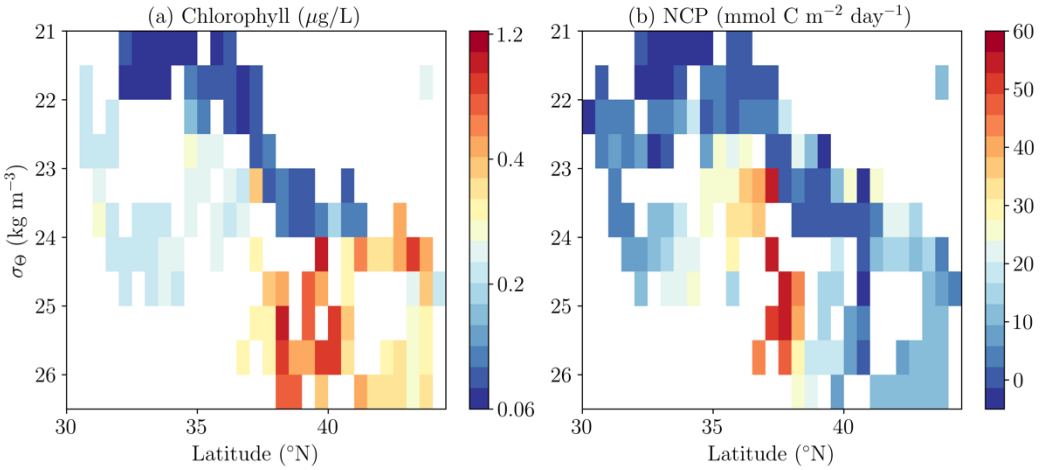

Figure 7. Bin-averaged a) CHL (μg L^{-1}) from the May and July cruises, and b) NCP (mmol C m^{-2} d^{-1}) from the May, July and September cruises, in latitude vs. σ_t space (note that CHL is shown on a $\log_{10}$ scale).

The overlap between the region of elevated NCP and the KE nutrient stream points to the importance of localized lateral and vertical nutrient supply within the KE jet in driving productivity in this region. However we do not find a similar overlap with the KE nutrient stream in the CHL data. This mismatch may, in part, be due to the more restricted set of CHL data skewing our results. However, annual climatologies of CHL in

this region show an increase with latitude, suggesting that even the data presented here is capturing consistent large-scale regional patterns in CHL. This result supports the hypothesis that NCP in the KE region is strongly controlled by both lateral and vertical nutrient supply within the jet. We would also expect to see seasonally driven differences in the coupling between CHL and NCP, and CHL and the nutrient stream. Future targeted studies in the KE region, with concurrent NCP and vertically resolved nutrient data, would make it possible to directly test this set of hypotheses.

3.6 (De)coupling between CHL and NCP

As mentioned above, one of the more striking results of this work is the strong seasonal and regional shift in the relationship between NCP and CHL, and the changing of the relationships of these variables to SLA. We see a strong decoupling between NCP and CHL in the May 2011 data (Figure 2a), with essentially no correlation ($r = 0.01$; $p < 0.05$) between NCP and CHL. In contrast, in the July data, NCP and CHL are very strongly correlated ($r = 0.85$; $p < 0.05$). Previous studies with concurrent NCP and CHL measurements have also found strong variations in the correlation between NCP and CHL. In high latitude systems, strong correlations between NCP and CHL were observed during the spring bloom [*Tortell and Long*, 2009], in summer [*Tortell et al.*, 2012], and across a springtime productivity hotspot at the transition between the coastal and open ocean [*Palevsky et al.*, 2013], but much weaker correlations after the peak of a bloom [*Tortell et al.*, 2011]. Conversely, a study in the equatorial Pacific found no correlation at all between NCP and CHL [*Stanley et al.*, 2010]. Previous studies have also demonstrated spatial decoupling between NCP and export of particles from the mixed layer [*Estapa et al.*, 2015], as well as 2-15 day temporal lags between peaks in surface CHL concentrations and in export flux [*Stange et al.*, 2017].

Regions with high NCP but low CHL concentrations (such as the region north of the KE axis in May 2011) could either reflect an early-phase bloom feature, where NCP is high but biomass has not yet had sufficient time to accumulate and produce high CHL concentrations, or could reflect an ecosystem where the majority of organic carbon produced is quickly exported from the mixed layer rather than accumulating biomass in

602 the surface. Similarly, regions with low NCP but high CHL concentrations could either
603 reflect a senescent bloom phase, where biomass remains high but NCP has diminished
604 due to a rise in respiration or decrease in primary production. Regions with both high
605 NCP and high CHL (such as the region north of the KE axis in July 2012) could reflect
606 an ecosystem where the majority of organic matter produced remains suspended in the
607 mixed layer rather than being exported, or an ecosystem with high export along with
608 significant biomass accumulation, although this latter scenario is probably less likely.
609 Future efforts to disentangle these potential explanations would benefit from
610 measurements of export below the mixed layer, and of particulate organic carbon and
611 phytoplankton community composition, since large cells that sink more quickly out of the
612 mixed layer may be more likely to contribute to export than to surface biomass
613 accumulation.
614
615 Although our study provides high spatial-resolution data across the KE region, each
616 cruise provides only a snapshot view of the system. As a result we cannot resolve
617 transient temporal contexts (e.g. bloom stage) that might influence the observed
618 relationships between NCP and CHL. Additionally, the KE jet is a strongly advective
619 system, with current speeds O(1 m s^{-1}). This combination of dynamic ecosystem
620 processes embedded within a strongly advective system likely plays an important role in
621 driving some portion of the observed decoupling between CHL and NCP.
622
623 **4. Conclusions**
624 In this study, we have investigated the distribution of O_2/Ar-derived NCP estimates in the
625 KE region with high resolution *in situ* underway data collected during spring, summer
626 and early fall. These observations reveal large spatial variability in NCP in the KE region
627 at all scales down to the submesoscale. We also find strong correlations between NCP
628 and SLA (a proxy for mesoscale eddies), but the sign of these correlations varies
629 seasonally and regionally. Several common threads emerge from our analysis. We find
630 that mesoscale dynamics consistently play an important role in modulating NCP. The KE
631 jet is a hotspot of NCP within the larger KE region, and high NCP is associated with the
632 same density and latitude range as the KE nutrient stream. Crucially, these observations

reveal the extent of fine scale synoptic variability in NCP within the KE region. This spatial and temporal variability is lost in large-scale climatological studies, where the KE region is subsumed within broader regional averaging. Resolving and understanding the drivers of this variability is likely to be key in building a mechanistic understanding of the range of factors controlling rates of NCP in the region, which ultimately will enable better parameterizations of these processes in Earth System Models.

Our observations also highlight seasonal and regional (de)coupling between NCP and CHL which may impact the accuracy of CHL-based estimates of productivity. Previous comparison of geochemical NCP estimates and satellite algorithm-based NCP in the North Pacific has shown that no single algorithm is applicable both in the subarctic and subtropical gyres [*Palevsky et al.*, 2016b], confounding the ability to use these algorithms to evaluate NCP across the Kuroshio Extension frontal region. Understanding the mechanisms that control the degree of coupling between NCP and CHL will allow us not only to better understand the processes controlling the biological carbon pump, but also to better predict NCP from observations of CHL and ocean color.

Although the results of this work suggest several avenues for further study, all require the development of methods for collecting sustained, high-resolution biogeochemical measurements within such dynamic western boundary current regions [*Todd et al.*, 2019]. Underway measurements collected from ships of opportunity provide a means of collecting data from repeat lines at high spatial resolution but are restricted to surface waters. In order to develop a mechanistic understanding of the physical and biological factors controlling NCP, it is key to observe not only the surface ocean, but also the vertical structure of the mixed layer, the photic zone, and the nutricline. We believe that the development and expansion of the Biogeochemical-Argo program [*Claustre et al.*, 2020; *Johnson et al.*, 2009] will be a key source of synoptic data on the vertical biogeochemical structure of the ocean. This study highlights the power of combining data collected from a range of observing platforms across different spatial and temporal ranges to build a fuller picture of this system. Future studies combining underway biogeochemical measurements from the ocean surface (e.g. ships of opportunity,

saildrones) with vertically resolved data derived from a range of platforms (e.g. floats, gliders) will drive developments in our mechanistic understanding of how biogeochemical processes in dynamic ocean regions are modulated by physical and biological controls.

5. Acknowledgements

All of the container ship transect data used in this study are available from the Biological & Chemical Oceanography Data Management Office (https://www.bco-dmo.org/project/626077). We thank the Orient Overseas Container Line (OOCL) and the captains and crew of the M/V OOCL Tokyo and M/V OOCL Tianjin for their assistance and gracious hospitality at sea, as well as Mark Haught and Johnny Stutsman for assistance with field sampling and laboratory measurements. Field work for this study was supported by the NOAA Climate Program Office (A10OAR4310088 to PDQ) and by NSF Ocean Sciences (1259055 to PDQ). SC was supported by a Moore/Sloan Data Science and Washington Research Foundation Innovation in Data Science postdoctoral fellowship. HIP was funded by a NDSEG Fellowship from the Office of Naval Research, a NSF Graduate Research Fellowship, an ARCS Foundation Fellowship, and by the Postdoctoral Scholar Program at the Woods Hole Oceanographic Institution, with funding provided by the Weston Howland Jr. Postdoctoral Scholarship. LT was supported by the NASA Ocean Surface Topography Science Team on grants NNX17AH56G and NNX13AH19G. The altimeter products were produced by Ssalto/Duacs and distributed by Aviso, with support from CNES (http://www.aviso.altimetry.fr/duacs/).

687 **References**

688 Abraham, E. R. (1998), The generation of plankton patchiness by turbulent stirring,
689 *Nature*, *391*(6667), 577-580, doi:10.1038/35361.

690 Bracco, A., S. Clayton, and C. Pasquero (2009), Horizontal advection, diffusion, and
691 plankton spectra at the sea surface, *Journal of Geophysical Research*, *114*(C2),
692 doi:10.1029/2007jc004671.

693 Cassar, N., B. a. Barnett, M. L. Bender, J. Kaiser, R. C. Hamme, and B. Tilbrook (2009),
694 Continuous high-frequency dissolved O2/Ar measurements by equilibrator inlet mass
695 spectrometry, *Analytical chemistry*, *81*(5), 1855-1864, doi:10.1021/ac802300u.

696 Castro-Morales, K., N. Cassar, D. R. Shoosmith, and J. Kaiser (2013), Biological
697 production in the Bellingshausen Sea from oxygen-to-argon ratios and oxygen triple
698 isotopes, *Biogeosciences*, *10*(4), 2273-2291, doi:10.5194/bg-10-2273-2013.

699 Chelton, D. B., R. A. DeSzoeke, M. G. Schlax, K. El Naggar, and N. Siwertz (1998),
700 Geographical variability of the first baroclinic Rossby radius of deformation, *Journal of*
701 *Physical Oceanography*, *28*(3), 433-460, doi:10.1175/1520-0485.

702 Claustre, H., K. S. Johnson, and Y. Takeshita (2020), Observing the Global Ocean with
703 Biogeochemical-Argo, *Ann Rev Mar Sci*, *12*, 23-48, doi:10.1146/annurev-marine-
704 010419-010956.

705 Clayton, S., T. Nagai, and M. J. Follows (2014), Fine scale phytoplankton community
706 structure across the Kuroshio Front, *J. Plankton Res.*, *36*(4), 1017-1030,
707 doi:10.1093/plankt/fbu020.

708 Craig, H., and T. Hayward (1987), Oxygen supersaturation in the ocean: Biological
709 versus physical contributions, *Science*, *235*, 199-202.

710 DeVries, T., F. Primeau, and C. Deutsch (2012), The sequestration efficiency of the
711 biological pump, *Geophysical Research Letters*, *39*, L13601-L13601,
712 doi:10.1029/2012GL051963.

713 Emerson, S., P. Quay, C. Stump, D. Wilbur, and M. Knox (1991), O2, Ar, N2 and 222Rn
714 in surface waters of the subarctic ocean: net biological O2 production, *Global*
715 *Biogeochem. Cycles*, *5*(1), 49-69.

716 Estapa, M. L., D. A. Siegel, K. O. Buesseler, R. H. R. Stanley, M. W. Lomas, and N. B.
717 Nelson (2015), Decoupling of net community and export production in the Sargasso Sea,
718 *Global Biogeochem. Cycles*, *29*, doi:10.1002/2013GB004579.Received.

719 Eveleth, R., N. Cassar, R. M. Sherrell, H. Ducklow, M. P. Meredith, H. J. Venables, Y.
720 Lin, and Z. Li (2017), Ice melt influence on summertime net community production
721 along the Western Antarctic Peninsula, *Deep-Sea Research Part II: Topical Studies in*
722 *Oceanography*, *139*, 89-102, doi:10.1016/j.dsr2.2016.07.016.

723 Garcia, H. E., and L. I. Gordon (1992), Oxygen solubility in seawater: Better fitting
724 solubility equations, *Limnol. Oceanogr.*, *37*(6), 1307-1312,
725 doi:10.4319/lo.1992.37.6.1307.

726 Giering, S. L., and M. P. Humphreys (2018), Biological Pump, *Encyclopedia of*
727 *Geochemistry, Encyclopedia of Earth Sciences Series, ed W. White.(Cham: Springer)*, 1-
728 6.

729 Guo, X. Y., X. H. Zhu, Y. Long, and D. J. Huang (2013), Spatial variations in the
730 Kuroshio nutrient transport from the East China Sea to south of Japan, *Biogeosciences*,
731 *10*(10), 6403-6417, doi:10.5194/bg-10-6403-2013.

732 Guo, X. Y., X. H. Zhu, Q. Wu, and D. J. Huang (2012), The Kuroshio nutrient stream
733 and its temporal variation in the East China Sea, *Journal of Geophysical Research:*
734 *Oceans*, *117*(C1), n/a-n/a, doi:10.1029/2011jc007292.

735 Hamme, R., and S. Emerson (2004), The solubility of neon, nitrogen and argon in
736 distilled water and seawater, *Deep Sea Res., Part I*, *51*(11), 1517-1528,
737 doi:10.1016/j.dsr.2004.06.009.

738 Hamme, R. C., et al. (2012), Dissolved O2/Ar and other methods reveal rapid changes in
739 productivity during a Lagrangian experiment in the Southern Ocean, *Journal of*
740 *Geophysical Research: Oceans*, *117*(C4), n/a-n/a, doi:10.1029/2011jc007046.

741 Henson, S. A., C. Beaulieu, and R. Lampitt (2016), Observing climate change trends in
742 ocean biogeochemistry: when and where, *Glob Chang Biol*, *22*(4), 1561-1571,
743 doi:10.1111/gcb.13152.

744 Honda, M. C., Y. Sasai, E. Siswanto, A. Kuwano-Yoshida, H. Aiki, and M. F. Cronin
745 (2018), Impact of cyclonic eddies and typhoons on biogeochemistry in the oligotrophic
746 ocean based on biogeochemical/physical/meteorological time-series at station KEO,
747 *Progress in Earth and Planetary Science*, *5*(1), doi:10.1186/s40645-018-0196-3.

748 Imai, K., Y. Nojiri, N. Tsurushima, and T. Saino (2002), Time series of seasonal
749 variation of primary productivity at station KNOT (44 oN, 155 oE) in the sub-arctic
750 western North Pacific, *Deep Sea Res., Part II*, *49*, 5395-5408.

751 Intergovernmental Oceanography Commission (1994), *Protocols for the Joint Global*
752 *Ocean Flux Study (JGOFS) Core Measurements*, UNESCO, Paris.

753 Izett, R. W., C. C. Manning, R. C. Hamme, and P. D. Tortell (2018), Refined estimates of
754 net community production in the Subarctic Northeast Pacific derived from ΔO2/Ar
755 measurements with N2O-based corrections for vertical mixing, *Global Biogeochemical*
756 *Cycles*, *32*(3), 326-350.

757 Johnson, K., W. Berelson, E. Boss, Z. Chase, H. Claustre, S. Emerson, N. Gruber, A.
758 Körtzinger, M. J. Perry, and S. Riser (2009), Observing Biogeochemical Cycles at Global

759 Scales with Profiling Floats and Gliders: Prospects for a Global Array, *Oceanography*,
760 *22*(3), 216-225, doi:10.5670/oceanog.2009.81.

761 Jonsson, B. F., S. C. Doney, J. Dunne, and M. Bender (2013), Evaluation of the Southern
762 Ocean O2/Ar-based NCP estimates in a model framework, *Journal of Geophysical*
763 *Research: Biogeosciences*, *118*(2), 385-399, doi:10.1002/jgrg.20032.

764 Kaiser, J., M. K. Reuer, B. Barnett, and M. L. Bender (2005), Marine productivity
765 estimates from continuous O2/Ar ratio measurements by membrane inlet mass
766 spectrometry, *Geophysical Research Letters*, *32*(19), 1-5, doi:10.1029/2005GL023459.

767 Kono, T., and M. Sato (2010), A mixing analysis of surface water in the Oyashio region:
768 Its implications and application to variations of the spring bloom, *Deep Sea Research*
769 *Part II: Topical Studies in Oceanography*, *57*(17-18), 1595-1607,
770 doi:10.1016/j.dsr2.2010.03.004.

771 Kouketsu, S., H. Kaneko, T. Okunishi, K. Sasaoka, S. Itoh, R. Inoue, and H. Ueno
772 (2015), Mesoscale eddy effects on temporal variability of surface chlorophyll a in the
773 Kuroshio Extension, *Journal of Oceanography*, *72*(3), 439-451, doi:10.1007/s10872-015-
774 0286-4.

775 Laws, E. A. (1991), Photosynthetic quotients, new production and net community
776 production in the open ocean, *Deep Sea Research*, *38*(1), 143-167.

777 Lévy, M., and P. Klein (2004), Does the low frequency variability of mesoscale dynamics
778 explain a part of the phytoplankton and zooplankton spectral variability?, *Proceedings of*
779 *the Royal Society A: Mathematical, Physical and Engineering Sciences*, *460*(2046),
780 1673-1687, doi:10.1098/rspa.2003.1219.

781 Lockwood, D., P. D. Quay, M. T. Kavanaugh, L. W. Juranek, and R. A. Feely (2012),
782 High-resolution estimates of net community production and air-sea CO2flux in the
783 northeast Pacific, *Global Biogeochemical Cycles*, *26*(4), n/a-n/a,
784 doi:10.1029/2012gb004380.

785 Mackas, D. L., K. L. Denman, and M. R. Abbott (1985), Plankton Patchiness - Biology in
786 the Physical Vernacular, *B Mar Sci*, *37*(2), 652-674.

787 Mahadevan, A. (2015), The Impact of Submesoscale Physics on Primary Productivity of
788 Plankton, *Ann Rev Mar Sci*, doi:10.1146/annurev-marine-010814-015912.

789 Manning, C. C., E. M. Howard, D. P. Nicholson, B. Y. Ji, Z. O. Sandwith, and R. H. R.
790 Stanley (2017), Revising estimates of aquatic gross oxygen production by the triple
791 oxygen isotope method to incorporate the local isotopic composition of water,
792 *Geophysical Research Letters*, 1-9, doi:10.1002/2017GL074375.

793 Matsumoto, K., O. Abe, T. Fujiki, C. Sukigara, and Y. Mino (2016), Primary productivity
794 at the time-series stations in the northwestern Pacific Ocean: is the subtropical station

795 unproductive?, *Journal of Oceanography*, *72*(3), 359-371, doi:10.1007/s10872-016-
796 0354-4.

797 Nagai, T., and S. Clayton (2017), Nutrient interleaving below the mixed layer of the
798 Kuroshio Extension Front, *Ocean Dynamics*, doi:10.1007/s10236-017-1070-3.

799 Nightingale, P. D., G. Malin, C. S. Law, A. J. Watson, P. S. Liss, M. I. Liddicoat, J.
800 Boutin, and R. C. Upstill-Goddard (2000), In situ evaluation of air-sea gas exchange
801 parameterizations using novel conservative and volatile tracers, *Global Biogeochem.*
802 *Cycles*, *14*(1), 373-387.

803 Palevsky, H. I., P. D. Quay, D. E. Lockwood, and D. P. Nicholson (2016a), The annual
804 cycle of gross primary production, net community production, and export efficiency
805 across the North Pacific Ocean, *Global Biogeochemical Cycles*, *30*(2), 361-380,
806 doi:10.1002/2015gb005318.

807 Palevsky, H. I., P. D. Quay, and D. P. Nicholson (2016b), Discrepant estimates of
808 primary and export production from satellite algorithms, a biogeochemical model, and
809 geochemical tracer measurements in the North Pacific Ocean, *Geophysical Research*
810 *Letters*, *43*(16), 8645-8653, doi:10.1002/2016gl070226.

811 Palevsky, H. I., F. Ribalet, J. E. Swalwell, C. E. Cosca, E. D. Cokelet, R. A. Feely, E. V.
812 Armbrust, and P. D. Quay (2013), The influence of net community production and
813 phytoplankton community structure on CO_2 uptake in the Gulf of Alaska, *Global*
814 *Biogeochem. Cycles*, *27*(3), 664-676, doi:10.1002/gbc.20058.

815 Qiu, B., S. Chen, N. Schneider, and B. Taguchi (2014), A Coupled Decadal Prediction of
816 the Dynamic State of the Kuroshio Extension System, *Journal of Climate*, *27*(4), 1751-
817 1764, doi:10.1175/jcli-d-13-00318.1.

818 Reuer, M. K., B. A. Barnett, M. L. Bender, P. G. Falkowski, and M. B. Hendricks (2007),
819 New estimates of Southern Ocean biological production rates from O2/Ar ratios and the
820 triple isotope composition of O2, *Deep Sea Res., Part I*, *54*, 951-974,
821 doi:10.1016/j.dsr.2007.02.007.

822 Rocha, C. B., S. T. Gille, T. K. Chereskin, and D. Menemenlis (2016), Seasonality of
823 submesoscale dynamics in the Kuroshio Extension, *Geophysical Research Letters*,
824 *43*(21), 11,304-311,311, doi:10.1002/2016gl071349.

825 Rosengard, S. Z., R. W. Izett, W. J. Burt, N. Schuback, and P. D. Tortell (2020),
826 Decoupling of ΔO 2/ Ar and particulate organic carbon dynamics in nearshore surface
827 ocean waters, *Biogeosciences*, *17*(12), 3277-3298.

828 Schmidtko, S., G. C. Johnson, and J. M. Lyman (2013), MIMOC: A global monthly
829 isopycnal upper-ocean climatology with mixed layers, *Journal of Geophysical Research:*
830 *Oceans*, *118*(4), 1658-1672, doi:10.1002/jgrc.20122.

831 Stange, P., L. T. Bach, F. A. C. Le Moigne, J. Taucher, T. Boxhammer, and U. Riebesell
832 (2017), Quantifying the time lag between organic matter production and export in the
833 surface ocean: Implications for estimates of export efficiency, *Geophysical Research*
834 *Letters*, *44*(1), 268-276, doi:10.1002/2016GL070875.

835 Stanley, R. H. R., J. B. Kirkpatrick, N. Cassar, B. A. Barnett, and M. L. Bender (2010),
836 Net community production and gross primary production rates in the western equatorial
837 Pacific, *Global Biogeochem. Cycles*, *24*, GB4001-GB4001, doi:10.1029/2009GB003651.

838 Strickland, J. D. H., and T. R. Parsons (1972), *A practical handbook of seawater*
839 *analysis.*, Second Edition ed., Fisheries Research Board of Canada Bulletin, Ottawa.

840 Todd, R. E., et al. (2019), Global Perspectives on Observing Ocean Boundary Current
841 Systems, *Frontiers in Marine Science*, *6*, doi:10.3389/fmars.2019.00423.

842 Tortell, P. D. (2005), Dissolved gas measurements in oceanic waters made by membrane
843 inlet mass spectrometry, *Limnol. Oceanogr.: Methods*, *3*, 24-37.

844 Tortell, P. D., E. C. Asher, H. W. Ducklow, J. A. Goldman, J. W. Dacey, J. J. Grzymski,
845 J. N. Young, S. A. Kranz, K. S. Bernard, and F. M. Morel (2014), Metabolic balance of
846 coastal Antarctic waters revealed by autonomous pCO2 and ΔO2/Ar measurements,
847 *Geophysical Research Letters*, *41*(19), 6803-6810.

848 Tortell, P. D., C. Guéguen, M. C. Long, C. D. Payne, P. Lee, and G. R. DiTullio (2011),
849 Spatial variability and temporal dynamics of surface water pCO2, ΔO2/Ar and
850 dimethylsulfide in the Ross Sea, Antarctica, *Deep Sea Research Part I: Oceanographic*
851 *Research Papers*, *58*(3), 241-259, doi:10.1016/j.dsr.2010.12.006.

852 Tortell, P. D., and M. C. Long (2009), Spatial and temporal variability of biogenic gases
853 during the Southern Ocean spring bloom, *Geophysical Research Letters*, *36*(1),
854 doi:10.1029/2008gl035819.

855 Tortell, P. D., M. C. Long, C. D. Payne, A.-C. Alderkamp, P. Dutrieux, and K. R. Arrigo
856 (2012), Spatial distribution of pCO2, ΔO2/Ar and dimethylsulfide (DMS) in polynya
857 waters and the sea ice zone of the Amundsen Sea, Antarctica, *Deep Sea Research Part II:*
858 *Topical Studies in Oceanography*, *71-76*, 77-93, doi:10.1016/j.dsr2.2012.03.010.

859 Ulfsbo, A., N. Cassar, M. Korhonen, S. V. Heuven, and M. Hoppema (2014),
860 Latesummernet communityproduction in the central Arctic Ocean using multiple
861 approaches Adam, *Global Biogeochemical Cycles*, *28*, 1129-1148,
862 doi:10.1002/2014GB004833.Received.

863 van Gennip, S., A. P. Martin, M. A. Srokosz, J. T. Allen, R. Pidcock, S. C. Painter, and
864 M. C. Stinchcombe (2016), Plankton patchiness investigated using simultaneous nitrate
865 and chlorophyll observations, *Journal of Geophysical Research: Oceans*,
866 doi:10.1002/2016jc011789.

867 Westberry, T. K., M. J. Behrenfeld, P. Schultz, J. P. Dunne, M. R. Hiscock, S.
868 Maritorena, J. L. Sarmiento, and D. A. Siegel (2016), Annual cycles of phytoplankton
869 biomass in the subarctic Atlantic and Pacific Ocean, *Global Biogeochemical Cycles*, *30*,
870 1-16, doi:10.1002/2015GB005276.Received.

871 Wong, C. S., N. A. D. Waser, Y. Nojiri, F. A. Whitney, J. S. Page, and J. Zeng (2002),
872 Seasonal cycles of nutrients and dissolved inorganic carbon at high and mid latitudes in
873 the North Pacific Ocean during the Skaugran cruises: determination of new production
874 and nutrient uptake ratios, *Deep Sea Res., Part II*, *49*, 5317-5338.
875